Al-Bahir Journal for Engineering and Pure Sciences
BJEPS

Volume 2 | Issue 2 Article 4

Effect of Spray Angle on Some Physical Properties of a Ceramic System Produced by Thermal spraying Coating

Waleed A. Salih
Physics Department, College Education of pure Science, KirkukUniversity, Kirkuk, Iraq

Sabah M. Aman Allah
Physics Department, College Education of pure Science, KirkukUniversity, Kirkuk, Iraq

Salih Y. Darweesh
Physics Department, College of Education TuzKhurmatu, Tikrit University, Tikrit, Iraq.

Follow this and additional works at: https://bjeps.alkafeel.edu.iq/journal

 Part of the Physical Sciences and Mathematics Commons

Recommended Citation

Salih, Waleed A.; Allah, Sabah M. Aman; and Darweesh, Salih Y. (2023) "Effect of Spray Angle on Some Physical Properties of a Ceramic System Produced by Thermal spraying Coating," *Al-Bahir Journal for Engineering and Pure Sciences*: Vol. 2: Iss. 2, Article 4.
Available at: https://doi.org/10.55810/2313-0083.1022

This Original Study is brought to you for free and open access by Al-Bahir Journal for Engineering and Pure Sciences. It has been accepted for inclusion in Al-Bahir Journal for Engineering and Pure Sciences by an authorized editor of Al-Bahir Journal for Engineering and Pure Sciences. For more information, please contact bjeps@alkafeel.edu.iq.

Effect of Spray Angle on Some Physical Properties of a Ceramic System Produced by Thermal spraying Coating

Cover Page Footnote

non

This original study is available in Al-Bahir Journal for Engineering and Pure Sciences: https://bjeps.alkafeel.edu.iq/journal/vol2/iss2/4

ORIGINAL STUDY

Effect of Spray Angle on Some Physical Properties of a Ceramic System Produced by Thermal Spraying Coating

Waleed A. Salih [a], Sabah M. Aman Allah [a], Salih Y. Darweesh [b,*]

[a] Physics Department, College Education of Pure Science, Kirkuk University, Kirkuk, Iraq
[b] Physics Department, College of Education TuzKhurmatu, Tikrit University, Tikrit, Iraq

Abstract

The angle of thermal spraying by the flame is considered one of the important influences on the coating layer, where alumina (Al_2O_3)% was used as a base material, and it was reinforced with two metals (TiAl) with weight ratios of (25%) in order to produce a cermet composite material with a final thickness ranging between (300−400) μm and with a fixed thermal spray distance of 16 cm, the samples resulting from the paint were thermally sintered at a temperature of (1000 °C) for an hour and a half, after the samples were taken out of the oven and some mechanical operation was performed on them, some physical tests were conducted, the most important of which included an examination X-ray diffraction, as well as porosity, hardness, and adhesion strength, to show through laboratory tests that the best thermal spray angle is 90°, at a mixing ratio of 25% after thermal sintering.

Keywords: Mechanical operation, Aluminum−titanium, Porosity, Adhesion strength

1. Introduction

Thermal spraying is a general term used to define a group of processes for depositing metallic or non-metallic materials in a molten or semi-molten state on substrates prepared in advance for the purpose of coating [1]. Thermal spraying results in coatings with good properties that give the sprayed surface high hardness and low wear rate [2,3]. As for the materials that are sprayed, they are in the form of powder, rods, or metal wires [4]. Painting materials that are in a solid state are heated, either by combustion of gases (such as flame spraying), or electrically by means of an electric arc, or an electric arc that heats and ionizes a stream of gases (plasma spray) [5]. . The coating material turns into a plastic or molten state when heated, then it is atomized and accelerated by gas pressure, which in turn transfers it to the base by forming a specific stream of droplets (the shape of the material during its transfer from the spray gun to the base). Thanks to the high gas impulse force, the droplets collide with the surface of the base and become flattened and stick to it, forming strips that are linked with the base and with each other, forming a lamellar coating [6,7]. Flame spraying technology is the most common type of thermal spraying in the world because of its simplicity and low cost [8]. In this technique, fuel gas combustion is used with oxygen as a source of heat required for melting paint materials [9]. Hydrogen, propane and acetylene gases are used as gaseous fuels, and acetylene gas is one of the commonly used gases due to its low risk in work, in addition to its availability and low cost [10]. The flame spraying technique generally gives coatings with acceptable properties despite the relatively low speed of molten particles approximately (1-50 ms^{-1}) and the low temperatures obtained from flame combustion (approximately 3000 °C) [11,12]. The flame temperature reaches about (2700 °C) [13,14]

Received 6 March 2023; revised 10 March 2023; accepted 10 March 2023.
Available online 3 April 2023

* Corresponding author.
E-mail addresses: wlydaljbwrb4@gmail.com (W.A. Salih), dr.sabah.phy.sc@tu.edu.iq (S.M. Aman Allah), Salih.younis@tu.edu.iq (S.Y. Darweesh).

https://doi.org/10.55810/2313-0083.1022
2313-0083/© 2023 University of AlKafeel. This is an open access article under the CC-BY-NC license (http://creativecommons.org/licenses/by-nc/4.0/)

and in the best conditions, when using an oxy-acetylene torch, it may reach (3100 °C) [15,16], which means that the use of spray materials is limited. The pressure of the combustion gases acts as a driving force for the particles and accelerates them to a speed (100 ms^{-1}) only [17]. The present article aims to study the variables of thermal spraying with flame, which included changing the angle of thermal spraying and its effect on the physical properties of the resulting coating.

2. Raw materials

Alumina was used as the base material produced by (CDH) company, of (Indian) origin, with a grain size of (100 μm) and purity (99.7%), while the reinforcement material was metallic (TiAl) produced by (Metco 110), of origin (American), with a grain size of (75 μm) and a purity of (99.9%). As for the basic binding material, it is (80%Al–20%Ni) produced by (Sulzer Metco) No. (443), of (Swedish) origin, with a grain size of (100 μm) and a purity of (99.9%).

3. Method of work

The sample preparation process (surface preparation) before thermal spraying is important for the success of the coating process, because the degree of adhesion of the coating materials to the surface of the substrate depends on the mechanical interlocking of the solidified particles at the surface of the substrate. After the samples are cut and softened, they are washed with alcohol to remove fat or any other contaminants, taking into account not to hold them by hand throughout the preparation period. A grit blasting device manufactured by the Swedish company (Sabtux) was used to increase the surface roughness of the samples. The granules used are silicon carbide or alumina granules with a range of diameters from 0.7 mm to 1.5 mm. The prepared Cermet Powder is sprayed towards the base of the coating through a spray gun type (GH-4/h) of Chinese origin. The mixing ratio of oxygen with acetylene can be determined through a special regulator (Flowmeter). A special clamp is designed to hold the spray gun. And install it with different spray distances (16 cm) towards the base of carrying samples. The best spraying parameters were chosen through conducting a series of preliminary experiments to ensure that coating layers with good adhesion strength and a certain thickness are obtained in order to qualify us to study the physical properties of this type of coating. Table 1 gives the spraying parameters used. The resulting paint samples were subjected to a thermal sintering process at (1000 °C) for an hour and a half, after which they were ready for physical examinations.

Table 1. Parameters of the flame thermal spraying process.

Oxy - Acetylene Mixing	4:0.7
Flame Spray Temp.	3000 °C
Spraying Distance	(16) cm
Rotation Number	4
Particle size of Powders	(75–100) μm
Coating Time	(1–2) min
Maximum Thickness Coating	(400) μm

4. Physical examinations

4.1. Scanning electron microscope

The scanning electron microscope is one of the most important electron microscopes in evaluating the topography of the surface, examining the surface structure and calculating the particle size. It is also possible to know the proportions of the constituent elements of the compound through (EDX), where a scanning electron microscope (MIRA3 TESCAN) of Belgian origin was used. Through it, a beam of electrons is shed on the atoms present in the surface of the sample, and thus several different signals are produced that give information about the shape and topography of the outer surface of the samples used [18].

4.2. Porosity

Porosity is considered the preferred alternative for considerations of some packing characteristics of powders, and it can be defined as the ratio of pores in powders to the bulk volume of the sample. Porosities are of three types, namely (closed pores, connected open pores, and separate open pores). [19], and there are several factors that affect the porosity, including the shape of the granules, their size and distribution, and the strength of the bonding between the granules has a great effect on the porosity. An increase in the fine granules relative to the coarse granules means a decrease in the porosity [20]. The pressure used for formation affects the proportion of the pores [21]; Because the use of high pressure will lead to an increase in compaction of granules and a decrease in porosity. The sintering temperature of the model, for

example, materials with low melting points within the structure will melt and fill the pores and reduce the porosity. The percentage of true porosity can be measured by the following relationship [22]:

$$\mathbf{T.P.\%} = \frac{\mathbf{T.D.} - \mathbf{B.D.}}{\mathbf{T.D.}} \times \mathbf{100\ \%} \quad (1)$$

Since: T.P.: Percentage of The Total Porosity of the Sample, B.D.: Sample Density in Practice (g/cm^3), T.D.: Theoretical Sinter Body Density (g/cm^3).

4.3. Hardness

A French Vickers Hardness measuring device was used. As 10 readings were recorded for one press (5 readings for each face of the press) in a radial manner from the center of the surface of the press to its periphery, and then the average of these readings was calculated, and the results of the readings were very close, indicating the homogeneity of the surface and the absence of almost any internal defects, the relationship shows Vickers hardness value [23].

$$\mathbf{Hv} = \frac{\mathbf{2}F\ Sin\ \mathbf{136^\circ/2}}{d} \approx \mathbf{1.854\ F/d^2} \quad (2)$$

It represents: F: The Amount of Load Imposed in N, d: The Average Impact Diameter in mm.

4.4. Adhesion strength

The adhesion measurement of the coating layer was carried out using a tensile device with a maximum load of (2 Ton) according to the standard (ASTM- (C633)) [24]. The adhesion samples were installed in the jaws of the tensioning device, as shown in Fig. 1. For the purpose of adhesion measurement, uncoated base material samples were prepared with an equal number of sprayed and unsprayed samples. Chemical cleaning operations were carried out by using alcohol to clean all samples in order to get rid of fat, dust and any other contaminants that hinder the process of gluing the two pieces together, after which an epoxy adhesive was used to stick the two pieces together (sprayed and not sprayed). A thin layer of adhesive is applied to the surface of the paint so that it covers all parts of the surface taking into account that it is uniform. Then the two pieces are pressed together for a period of (1hr) and then placed in a drying oven for a period of (24hrs) at a temperature of (50 °C). Before conducting the tensile test, the adhesion must be uniform and the tensile force applied when conducting the test should be perpendicular to the surface of the coating. After the sample is installed in the tensioning device, a tensile load is applied to each test sample at a tensile rate of (1 mm/min) until the sample fails, as the highest applied load is recorded.

5. Results and discussion

5.1. Effect of spray angle on Vickers hardness of cermet coatings

We notice through Fig. 2, which shows the relationship between the spray angle (TiAl) and the Vickers hardness before and after the thermal

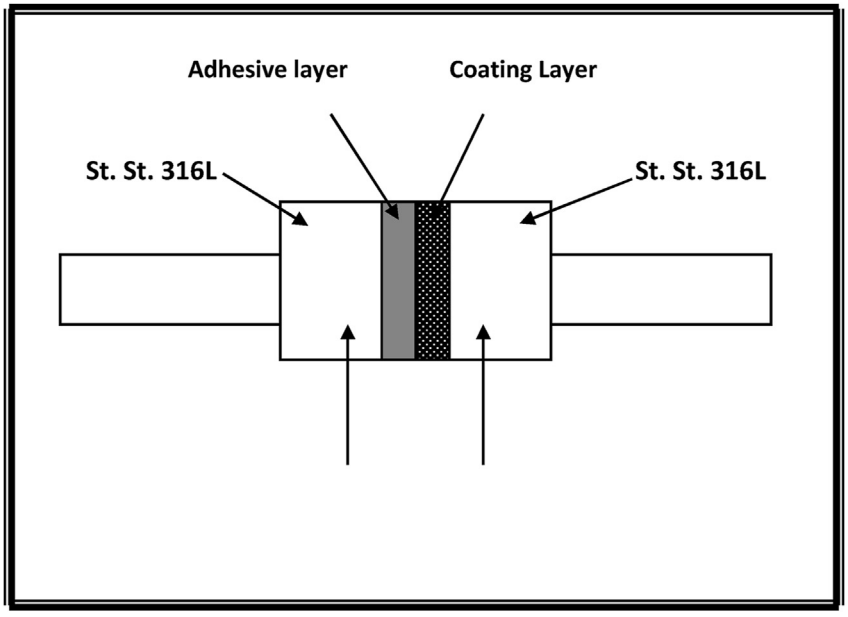

Fig. 1. Adhesion samples are installed in the adhesion device.

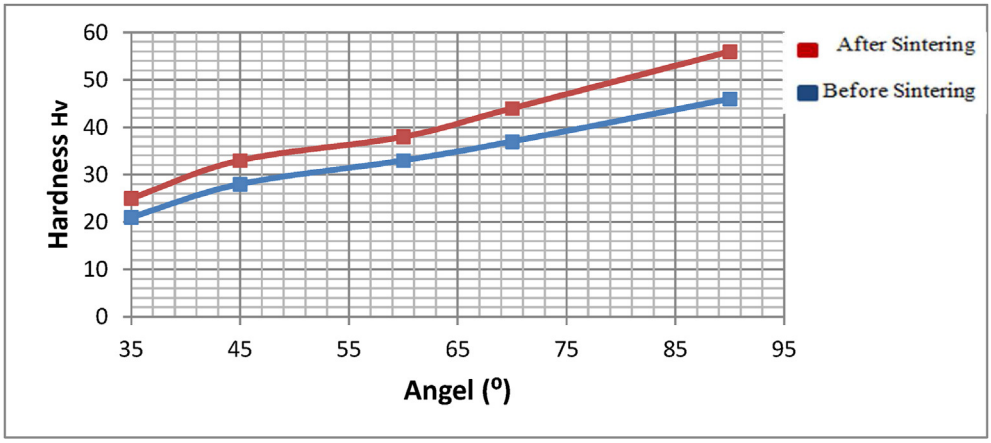

Fig. 2. Shows the relationship between spray angle and Vickers hardness before and after sintering.

sintering process at a temperature (1000 °C) and the time is an hour and a half, as we notice through the figure when the spray angle increases, the hardness value increases, so we note At (35º), the hardness value is (221 kg/mm^2) before sintering and (225 kg/mm^2) after sintering, while the hardness value at (90º) is (246 kg/mm) before sintering and (256 kg/mm) after sintering. This is until at very few angles the paint will gather at a specific area without the rest of the areas and agglomeration will occur and then the coating will fall partially as well as cracks will occur and thus the porosity will increase and the hardness will decrease, but at large angles the coating will get gatherings and you will get the same conditions as the few corners, While the angle (90º) we notice obtaining almost distinctive physical properties, as we note the regularity and consistency of the surface layer, which gave good values for the physical properties [24].

5.2. The effect of spray angle on the porosity of the ceramic coating

We notice through Fig. 3, which shows the relationship between the effect of the angle and the porosity of the coating before and after the thermal sintering process at a temperature of (1000 °C) for an hour and a half, we notice through the figure when the spray angle increases, the porosity value decreases, so we notice at (35º) The value of porosity is (22.2%) before sintering and (16.5%) after sintering, while the value of porosity at (90º) is (11.5%) before

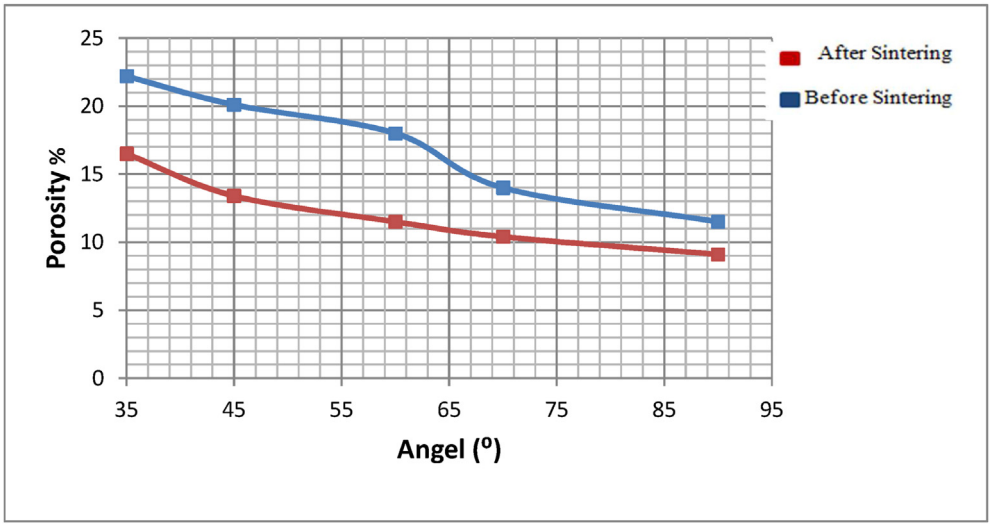

Fig. 3. Illustrates the relationship between spray angle and coating porosity.

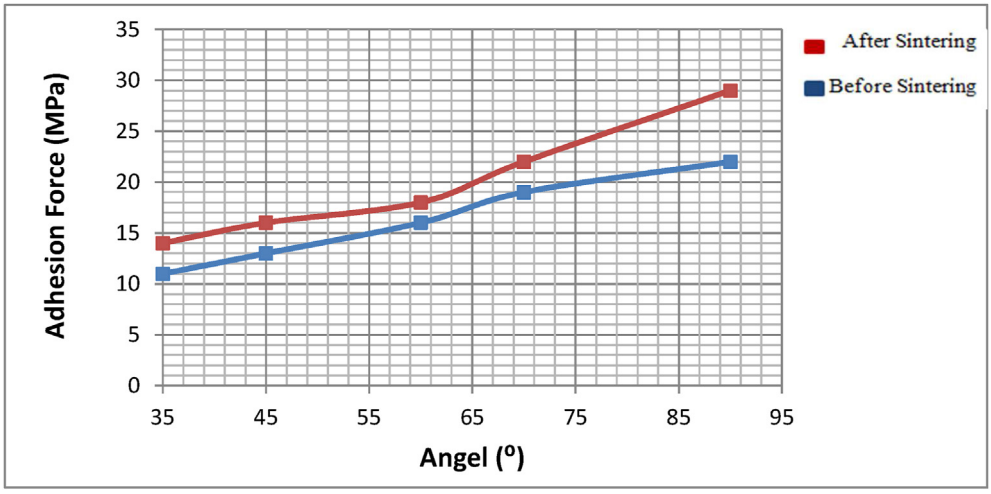

Fig. 4. Shows the relationship between spray angle and adhesion force.

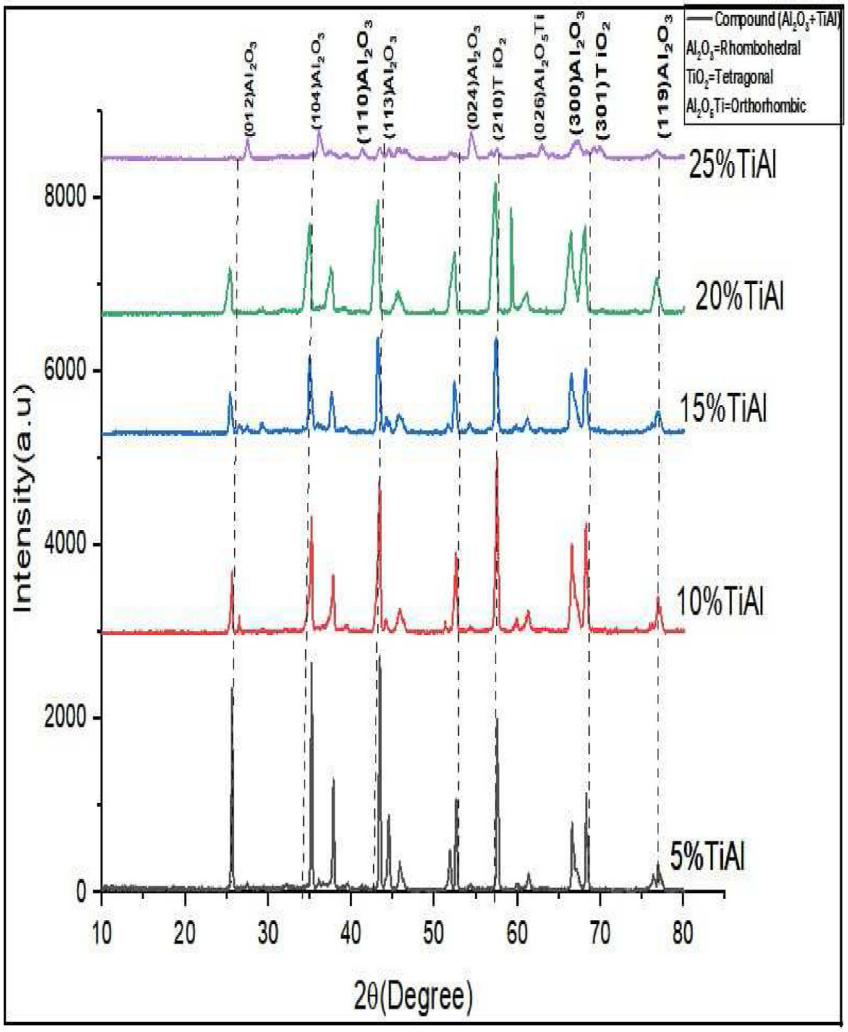

Fig. 5. Shows the diffraction of X-rays at different reinforcement concentrations (5%, 10%, 15%, 20%, 25%) after thermal sintering at an angle of 90°.

sintering and (9.1%) after sintering. From the spray gun to the base of the paint is random, which leads to the occurrence of agglomerations and aggregations of the paint in certain areas and thus the pores increase, while we notice at the angle of 90° there is consistency and flatness of the cermet coating, which in turn gave valuable physical results, and the scattering of the molten droplets at small angles is large very [25,26].

5.3. The effect of spray angle on the adhesion strength of cermet coatings

We notice through Fig. 4, which shows the relationship between the effect of the angle (TiAl) and the adhesion strength before and after the thermal sintering process at a temperature of (1000 °C) for an hour and a half, we notice through the figure when the spray angle increases, the adhesion value increases, so we note at (35º), the adhesion strength value is (11 MPa) before sintering and (14 MPa) after sintering, while the adhesion value at (90º) is (14 MPa) before sintering and (29 MPa) after sintering, and the first thing that made an increase in the adhesion strength With the angle of spraying, this is due to an increase in the homogeneity and bonding of the coating layers, because the heat leads to shrinking and reducing the pores, which leads to an increase in the homogeneity between the parts of the coating. The large atoms convergence and homogeneity are thus improved by the composition of the coating material [27,28].

5.4. X-ray diffraction (XRD) results

Fig. 5 shows the X-ray diffraction of titanium-aluminium-supported weight ratio concentrations (5%, 10%, 15%, 20%, 25%), respectively. As we notice through the figure, i.e. 5% reinforcement, we find the appearance of alumina (Al2O3) with a triple crystal system (rhombohedral lattice system) clear during the composition, which appeared at angle values (26 = θ2) as well as (44, 35 = θ2) and other angle values, as well The appearance of titanium in an oxidized form by (TiO2) as a result of heat and in a tetragonal crystal system at angle values (44.5, 62,69 = θ2) and at other angle values. Thus, we find that the action of temperature has a significant effect on the homogeneity of the crystal structures with each other, as well as the oxidation of each Made of titanium and aluminum, each of which appears in its oxide form, which has high durability and hardness. At 25%, we notice the beginning of a greater spread of the reinforcement powder with a decrease in the peaks of the alumina structures, as we notice as a result of increasing the reinforcement ratios, the phase (Al2O5 Ti) appears with an orthorhombic crystal system, which is characterized by high durability and hardness that enables it to withstand high temperatures, which It continues to appear with an increase in the reinforcement ratios (TiAl), and thus this ratio was relied upon for the rest of the physical examinations [29–31].

6. Conclusions

Important methods through which many industrial applications that suffer from external cracking or peeling can be treated, for example turbine blades and oil pipes, where the important conclusion from the current article is the possibility of strengthening an oxide material such as alumina with a metal material, which is (TiAl). And with different weight ratios of the reinforcement material, then relying on a percentage of 25%, and a spray distance of 16 cm. Then it was found that the hardness value is (56 kg/mm^2), the porosity is (9.1%), and the adhesion strength is (29 MPa) after thermal sintering, while the results of X-ray diffraction gave that the best thermal spray angle is 90°, with a mixture of 25%.

Conflict of interest

No conflict of interest.

References

[1] Meierhofer F, Fritsching U. Synthesis of metal oxide nanoparticles in flame sprays: review on process technology, modeling, and diagnostics. Energy Fuel 2021;35(7):5495–537. https://doi.org/10.1021/acs.energyfuels.0c04054.
[2] Dorfman M. Thermal spray coatings. In: Handbook of environmental degradation of materials. William Andrew Publishing; 2018. p. 469–88. https://doi.org/10.1016/B978-0-323-52472-8.00023-X.
[3] Fauchais P, Vardelle A. Thermal sprayed coatings used against corrosion and corrosive wear. Adv Plasma Spray Appl 2012;10:34448.
[4] Boulos M, Fauchais P, Heberlein J. Thermal spray fundamentals: from powder to part. Springer; 2021.
[5] Gonzalez R, Ashrafizadeh H, Lopera A, Mertiny P, Mcdonald A. A review of thermal spray metallization of polymer-based structures. J Therm Spray Technol 2016;25:897–919. https://doi.org/10.1007/s11666-016-0415-7.
[6] Nouri A, Sola A. Powder morphology in thermal spraying. J Adv Manuf Proc 2019;1(3):e10020. https://doi.org/10.1002/amp2.10020.
[7] Boronenkov V, Korobov Y. Fundamentals of arc spraying. Physical and chemical regularities. Berlin/Heidelberg, Germany: Springer; 2016.

[8] Vardelle A, Moreau C, Themelis N, Chazelas C. A perspective on plasma spray technology. Plasma Chem Plasma Process 2015;35:491–509. https://doi.org/10.1007/s11090-014-9600-y.
[9] Sunitha K, Vasudev H. A short note on the various thermal spray coating processes and effect of post-treatment on Ni-based coatings. Mater Today Proc 2012;50:1452–7. https://doi.org/10.1016/j.matpr.2021.09.017.
[10] Kahar S, Singh A, Vala U, Desai A, Smit S. Thermal sprayed coating using zinc: a review. IRJET 2020;7(6):6497–503.
[11] Liao T, Biesiekierski A, Berndt C, King P, Ivanova P, Thissen H, et al. Multifunctional cold spray coatings for biological and biomedical applications: a review. Prog Surf Sci 2022:100654. https://doi.org/10.1007/s12647-022-00597-8.
[12] Sauter M, Roth A, Grebhardt A, Killinger A. High velocity flame spraying of highly-filled ceramic—polymer filaments (F-HVOF). Surf Coating Technol 2023;2023:129324. https://doi.org/10.1016/j.surfcoat.2023.129324.
[13] Berger L. Application of hardmetals as thermal spray coatings. Int J Refract Metals Hard Mater 2015;49:350–64. https://doi.org/10.1016/j.ijrmhm.2014.09.029.
[14] Sadeghi E, Markocsan N, Joshi S. Advances in corrosion-resistant thermal spray coatings for renewable energy power plants. Part I: effect of composition and microstructure. J Therm Spray Technol 2019;28:1749–88. https://doi.org/10.1007/s11666-019-00938-1.
[15] Vardelle A, Moreau C, Akedo J, Ashrafizadeh H, Berndt C, Berghaus J, et al. The 2016 thermal spray roadmap. J Therm Spray Technol 2016;25:1376–440. https://doi.org/10.1007/s11666-016-0473-x.
[16] Fauchais P, Heberlein J, Boulos M. Thermal spray fundamentals: from powder to part. Springer Science & Business Media; 2014. https://doi.org/10.1007/s11666-016-0473-x.
[17] Yang X, Shang W, Lu H, Liu Y, Yang L, Tan R, et al. An agglutinate magnetic spray transforms inanimate objects into millirobots for biomedical applications. Sci Robot 2020;5(48):eabc8191. https://doi.org/10.1126/scirobotics.abc8191.
[18] Prasad C, Joladarashi S, Ramesh M. Comparative investigation of HVOF and flame sprayed CoMoCrSi coating. AIP Conf Proc AIP Pub LLC 2020 July;2247(1):050004. https://doi.org/10.1063/5.0003883.
[19] Wong W, Vo P, Irissou E, Ryabinin A, Legoux J, Yue S. Effect of particle morphology and size distribution on cold-sprayed pure titanium coatings. J Therm Spray Technol 2013;22:1140–53. https://doi.org/10.1007/s11666-013-9951-6.
[20] Azizpour M, Tolouei-Rad M. The effect of spraying temperature on the corrosion and wear behavior of HVOF thermal sprayed WC-Co coatings. Ceram Int 2019;45(11):13934–41. https://doi.org/10.1016/j.ceramint.2019.04.091.
[21] Khamsepour P, Oberste-Berghaus J, Aghasibeig M, Ettouil F, Dolatabadi A, Moreau C. The effect of spraying parameters of the inner-diameter high-velocity air–fuel (ID-HVAF) torch on characteristics of Ti-6Al-4V in-flight particles and coatings formed at short spraying distances. J Therm Spray Technol 2023:1–18. https://doi.org/10.1007/s11666-023-01535-z.
[22] Salih E, Allah S, Darweesh S, Mohammed H. Study of some of the physical variables of a metal-based system using the powder method. J Phys: Conf Ser IOP Pub September 2021;1999(1):012068. https://doi.org/10.1088/1742-6596/1999/1/012068.
[23] Tan R. Development of alumina based feedstock for fused deposition modelling 3D printer (doctoral dissertation, UTAR). 2020. http://eprints.utar.edu.my/id/eprint/4113.
[24] Bahbou M, Nylén P, Wigren J. Effect of grit blasting and spraying angle on the adhesion strength of a plasma-sprayed coating. J Therm Spray Technol 2004;13:508–14. https://doi.org/10.1361/10599630421406.
[25] Tillmann W, Khalil O, Baumann I. Influence of direct splat-affecting parameters on the splat-type distribution, porosity, and density of segmentation cracks in plasma-sprayed YSZ coatings. J Therm Spray Technol 2021;30:1015–27. https://doi.org/10.1007/s11666-021-01180-4.
[26] Huang W, Zeng N, Zhong R, Zhou X, Zhu L. Effects of critical plasma spraying parameters on microstructure and mechanical properties of LaPO4-8YSZ thick composite coatings. J Alloys Compd 2023;938:168688. https://doi.org/10.1016/j.jallcom.2022.168688. 2023.
[27] Yasir Asaad S, Hussein Basheer M, Hameed Ammar S, Ridha Noor J, Alosfur Firas K Mohamad, Tahir Khawla J. Design and fabrication of A low-cost dip coating system for depositing homogeneous and transparent Zno thin films. Al-Bahir J Eng Pure Sci 2022;1(2). Article 2. Available at: https://doi.org/10.55810/2312-5721.1008.
[28] Darweesh S, Ali A, Khodair Z, Majeed Z. The effect of some physical and mechanical properties of cermet coating on petroleum pipes prepared by thermal spray method. J Fail Anal Prev 2019;19:1726–38. https://doi.org/10.1007/s11668-019-00772-1.
[29] Vijay V, Santhy K, Sivakumar G, Rajasekaran B. Thermal expansion and microstructure evolution of atmospheric plasma sprayed NiCrAlY bond coat using in-situ high temperature X-ray diffraction. Surf Coating Technol 2023;452:129132. https://doi.org/10.1016/j.surfcoat.2022.129132.
[30] Rachidi R, El Kihel B, Delaunois F. Microstructure and mechanical characterization of NiCrBSi alloy and NiCrBSi-WC composite coatings produced by flame spraying. Mater Sci Eng, B 2019;241:13–21. https://doi.org/10.1016/j.mseb.2019.02.002.
[31] Ali Wissam Abbas, Mihsen Hayder Hamied, Guzar Sajid H. Novel derivative for dithiocarbamite containing A new sulphur-Azo linkage and its complexes with Sn(II), Sn(IV), Co(II), Ni(II) and Cu(II) ions; synthesis, characterization and antibacterial activity. Al-Bahir J Eng Pure Sci 2023;2(1). Article 3. Available at: https://doi.org/10.55810/2312-5721.1016.